Hindawi Publishing Corporation
Applied and Environmental Soil Science
Volume 2012, Article ID 535646, 12 pages
doi:10.1155/2012/535646

Research Article

Investigations into Soil Composition and Texture Using Infrared Spectroscopy (2–14 μm)

Robert D. Hewson,[1] Thomas J. Cudahy,[2] Malcolm Jones,[3] and Matilda Thomas[4]

[1] *School of Mathematical and Geospatial Sciences, RMIT University, GPO Box 2476, Melbourne, VIC 3001, Australia*
[2] *CSIRO Earth Science and Resource Engineering, P.O. Box 1130, Bentley, WA 6102, Australia*
[3] *Geological Survey of Queensland, Level 10, 119 Charlotte Street, Brisbane, QLD 4000, Australia*
[4] *Geoscience Australia, GPO Box 378, Canberra, ACT 2601, Australia*

Correspondence should be addressed to Robert D. Hewson, robert.hewson@rmit.edu.au

Received 17 February 2012; Accepted 27 August 2012

Academic Editor: Sabine Chabrillat

The ability of thermal and shortwave infrared spectroscopy to characterise composition and texture was evaluated using both particle size separated soil samples and natural soils. Particle size analysis and separation into clay, silt, and sand-sized soil fractions was undertaken to examine possible relationships between quartz and clay mineral spectral signatures and soil texture. Spectral indices, based on thermal infrared specular and volume scattering features, were found to discriminate clay mineral-rich soil from mostly coarser quartz-rich sandy soil and to a lesser extent from the silty quartz-rich soil. Further investigations were undertaken using spectra and information on 51 USDA and other soils within the ASTER spectral library to test the application of shortwave, mid- and thermal infrared spectral indices for the derivation of clay mineral, quartz, and organic carbon content. A nonlinear correlation between quartz content and a TIR spectral index based on the 8.62 μm was observed. Preliminary efforts at deriving a spectral index for the soil organic carbon content, based on 3.4–3.5 μm fundamental H–C stretching vibration bands, were also undertaken with limited results.

1. Introduction

Mapping and analysing soils for their composition and textural characteristics typically involves extensive field work and laboratory techniques that are traditionally time consuming. However the measurement and determination of soil texture and composition is important for the mapping of areas vulnerable to soil erosion, driven by water and wind. Coarser-textured soils are more resistant to detachment and transport via raindrops, thus less affected to water-assisted erosion [1]. Soils with a silt content above 40% are considered highly erodible while clay particles can potentially combine with organic matter to form aggregates or clods which assist in their resistance to erosion [1]. Also, studies of the critical shear wind velocities required for transportation of different-sized soil particles indicate, those with diameters between 0.10 to 0.15 mm are the most vulnerable to wind erosion [1].

Another motivation to determine a soil's texture and composition, including mineralogy, is with the aim to measure a soil's ability to retain water or enable drainage. Clay minerals such as montmorillonite can exhibit swelling behaviour, absorbing and storing water, within their layered lattice structure [2]. Such finer textured clay rich soils can offer more water for plant growth than sandy soils. Sandy soils are more vulnerable to drought than clayey soils, storing less water and likely to lose water more rapidly by the growing plants [3]. However under flood conditions, clay rich soils exhibit poor drainage of excess water and may become waterlogged.

The incorporation of spectrally derived textural and compositional information into soil classification schemes will be particularly undertaken for special-purpose classification with specific aims, such as mapping erodibility [3]. White [2] describes the usefulness of texture classification of soils for drought vulnerability and poor aeration.

In addition, estimation of surface soil texture and the identified presence or absence of certain minerals is still potentially an important input for general-purpose soil classification based on quantifiable properties that define its morphology, as distinct from its genesis. Soil classification in the USA and Australia use mostly such soil morphology as a basis for classification although this also requires observing properties varying with depth and horizons [2]. Incorporating spectroscopy information into a comprehensive 3D morphology description therefore requires the use of proximal spectral measurements of excavated soil samples.

The overall interest to determine a soil's texture and composition can be summarized also by the need to monitor and map areas vulnerable to desertification, typically demonstrated by increased soil erosion. A detailed study by [3] examined the key indicators of desertification, including soil properties, with the aim of mapping areas vulnerable to future desertification. The study described the soil parameter, erodibility, as primarily a property of the soil texture, with highest values for fine sand and silty soils with low clay content, but which can be decreased significantly with the presence of organic carbon matter [3]. With the world population expected to reach 9 billion by 2050, food security is an issue that can least afford the effects of erosion and desertification, reducing the existing arable agricultural land to feed a growing world [4].

Both proximal and remote sensing spectroscopy offers the potential of increasing the speed, and reducing the cost of interpreting soil samples for texture and composition. Recently, hyperspectral airborne imaging spectroscopy has been successfully applied to study some soil properties utilising electromagnetic radiation (EMR) within the visible-near infrared (VNIR) wavelengths (0.4–1.0 μm) and shortwave infrared (SWIR) wavelength regions (1.0–2.5 μm) [5]. Also, developments in airborne hyperspectral mid and thermal infrared remote sensing [6, 7] indicate the potential for mapping and characterising *in situ* soils. In the laboratory, thermal Infrared (TIR) spectroscopy within the 7–14 μm wavelength region has also shown its potential to provide soil mineralogy and textural information [8, 9]. In addition, several key organic carbon rich components (including lignin and cellulose) display diagnostic features related to the fundamental hydrocarbon H–C stretching vibration bands between 3.4 and 3.5 μm of the Mid Infrared (MIR) wavelength (3–5 μm) region [10, 11]. Spectral libraries, consisting of bidirectional TIR reflectance measurements, reveal diagnostic absorption features of many silicate minerals [9] although directional effects preclude their use for quantifiable comparison with TIR remote sensing signatures. Proximal laboratory spectral measurements within the visible-near infrared (VNIR) wavelengths (0.4–1.0 μm) and shortwave infrared (SWIR) wavelengths (1.0–2.5 μm) can identify ferric iron oxides, clay (AlOH), sulphates, and carbonate minerals [12] common within soils. However discriminating the quartz or silicate content of soils requires spectroscopy within the MIR region [11], and more commonly, the TIR region [9]. Table 1 summarises these wavelength regions containing diagnostic spectral signatures. Quantifying soil composition and characteristics has also been achievable using diffuse reflectance mid infrared (DRIFTS) spectroscopy techniques with the assistance of partial least squares calibration using a set of control soil samples [13]. However the physics of DRIFTS measurements and sampling operation precludes the conversion of the recorded reflectance signatures to absolute emissivities. The DRIFTS technique requires samples to be ground to a fine-powdered fraction (e.g., <80 μm) held in a small cap-like container from which reflectance and transmitted signatures are detected [14].

Proximal and remote sensing bidirectional VNIR-SWIR reflectance measurements can be approximately representative if soils are lambertion (e.g., isotropic for EMR). This assumption will not be suitable for anisotropic surfaces such as clay-dominated scalds. Ideally the comparison of MIR and TIR remote sensing with soil spectroscopy requires directional hemispherical reflectance (DHR) or emission mode proximal measurements of soils. Salisbury [15] demonstrated that for typical terrestrial materials with lambertian surfaces, it is possible to assume Kirchoff's Law ($\varepsilon = 1 - \rho$, where ε = emissivity and ρ = reflectance), enabling DHR and emissivity spectral signatures to be interchangeable. Later investigations within the 3–14 μm wavelength range have indicated that the change in emissivity with observation angle is small for all soils except for sand, where a change of up to 4% occurs within the 8–10 μm wavelength region [16].

Studies to interpret multispectral ASTER (Advanced Spaceborne Thermal Emission Reflectance Radiometer) TIR and airborne TIMS (Thermal Infrared Multispectral Scanner) imagery for soil mineralogy and texture however have demonstrated that their limited spatial and spectral resolution restricts this application [17]. Other studies have in particular described the difficulties of comparing heterogeneities within ASTER's 90 m pixel footprint with temperature and emissivity variability on the ground [18]. ASTER imagery has been available since 2000, with only five bands between 8.3 and 11.3 μm acquired for each 90 metre pixel. NASA's future HyspIRI spaceborne sensor will acquire at a slightly higher resolution of six TIR bands between 8.3 and 12.0 μm acquired for each 60 metre pixel [19].

Proximal DHR or high spectral resolution emission/radiance measurements are required to undertake soil spectroscopy to simulate passive hyperspectral MIR/TIR remote sensing techniques. Although extracting emissivity information from MIR/TIR remote sensing radiance imagery, particularly daytime (e.g., sunlit) MIR, is non trivial, several algorithms have been developed and applied [20, 21]. In this study, the derivation of selected compositional and textural soil information is targeted using key spectral absorption features within the 2 to 14 μm wavelength region as a pilot investigation for future hyperspectral infrared remote sensing applications.

The routine acquisition of hyperspectral TIR imagery is still at an early stage by airborne sensors such as the Spatially Enhanced Broadband Array Spectrograph System (SEBASS) with 128 bands between the 7.6 and 13.5 μm wavelengths [22]. Effectively at present, high-resolution spectral and spatial thermal infrared imagery is limited to

Table 1: Accessible windows within infrared spectral regions and their diagnostic compositional elements commonly found in soils.

SWIR 1.0–2.5 μm	MIR 3–5 μm	TIR 7–14 μm
Clay minerals (e.g., kaolinite, illite, montmorillonite), sulphates (e.g., gypsum) and carbonate (e.g., calcite) minerals	Organic carbon (e.g., lignin, cellulose), quartz, kaolinite	Quartz (including silt versus coarse sand), kaolinite, illite/montmorillonite, cellulose.

targeted airborne acquisitions or spot *in situ* or sampled-soil measurements. Until more routine and operational airborne (or higher resolution satellite) sensors are available, it is hoped that the use of field spectrometry or laboratory measurements of soil samples will be of use for some faster textural and compositional analysis than traditional laboratory techniques.

The possibility of undertaking three-dimensional soil spectroscopy is feasible using trays that are already currently used to store multiple small samples from regular depth intervals. Spectral sensing of rock chip trays are already used to acquire proximal VNIR-SWIR measurements of samples collected as part of routine mining and exploration drilling programs (http://www.csiro.au/en/Organisation-Structure/Divisions/Earth-Science–Resource-Engineering/HyChips.aspx). Laboratory VNIR-SWIR and potentially TIR measurements of such trays could be undertaken assuming the soil samples are sufficiently and consistently dried, and completely fill each tray compartment. A small field of view would be required to ensure there was no spectral interference with the tray container material or that no potential blackbody cavity effect was detected if utilizing a TIR emission mode spectrometer.

Initially this study was part of a much larger CSIRO-ESRE (Commonwealth Scientific Industrial Research Organisation, Division of Earth Science and Resource Engineering) project to map surface minerals/chemistries using airborne hyperspectral and satellite ASTER imagery, applying visible-near infrared and shortwave infrared sensing (proximal and airborne) techniques [23, 24]. The Tick Hill soils described and used in this paper were part of this CSIRO-ESRE study and collected within north Queensland (21°35′S, 139°55′E) (Figures 1 and 2). The good soil exposure and variability within this regional project area made this a useful study area for soil mapping via remote sensing and spectroscopy. Preliminary results of the TIR spectroscopy investigations undertaken for these Tick Hill soils were presented at the 19th World Congress of Soil Science [25]. This publication describes these results in greater detail, and in combination with more results from DHR measurements of USDA (United States Department of Agriculture) soil samples, available via the ASTER Spectral Library (ASL) [26] (http://speclib.jpl.nasa.gov/search-1/soil). Previous investigations of these USDA ASL spectra had found them useful for direct comparisons with field measurements when convolved to ASTER's 5 band TIR emissivity spectral resolution [27]. The ASL spectra within this study also included ten additional soil samples from a semiarid environment, Fowlers Gap, in western New South Wales, Australia, collected and analysed as part of a Ph.D. [28]. In addition, this investigation also incorporates further interpretation of short wavelength infrared (SWIR) spectroscopy for clay mineral content of all the examined Tick Hill samples.

2. Data and Laboratory Methods

2.1. Traditional Analytical Methods. In the past, texture has been assessed qualitatively in field soil surveys by moistening a sample with water and kneading between fingers and thumb until the aggregates are broken down and the soil grains thoroughly wetted [2]. More accurate quantitative but time consuming laboratory analysis of texture are also available by particle-size analysis using sedimentation techniques based on the rate of settling within a soil-water suspension [29]. Likewise traditional compositional analytical techniques involving X-ray diffraction are time consuming and expensive. It should be noted that in this spectroscopy study, "clay" content refers to clay mineral content (e.g., kaolinite, montmorillonite, and illite), that is, less than 2 μm, if disaggregated. Care is therefore required when comparing spectrally derived clay mineral content with particle size clay content as the determined 2 μm and finer fraction may include fine iron oxides or organic material if not properly pretreated [29].

2.2. Tick Hill Samples. Eight Tick Hill soil samples were chosen and analysed for International System particle size fractions [2], clay (<2 μm), silt (2–20 μm) and sand (20 μm–2 mm), by CSIRO land and water (http://www.clw.csiro.au/services/analytical/), using the traditional pipette method [29] (Table 2). According to the Australian Soil Resource Information System (ASRIS) mapping [2, 31], all except one sample used in this study area, were Ferrosols (Table 2), being high in free iron oxide content and low textural contrast between A and B horizons [30]. MI132 was mapped as a Tenosols with weak pedologic structure apart from the A horizon [30]. However at the detailed scale sampled in this Tick Hill area, a much greater diversity of soil properties were observed (Figure 1). These samples were firstly prepared by chemically removing salts, organic matter, and ferric iron [29]. These fractions were separated and dried for later spectral measurements. The resulting sand fraction was also further separated between 20–60 μm and 60 μm–2 mm, and dried for later spectral measurements.

The original raw soil and also four particle size fractions (<2 μm, 2–20 μm, 20–60 μm, 60 μm–2 mm) of each of the eight Tick Hill samples, were measured for their TIR spectral emissivity signatures using the Designs and Prototypes

Table 2: Tick Hill soil sample particle analysis results using Method code 517.08 of [29] where Fe/Al oxides, organic matter, and soluble salts are removed.

Sample	Clay <2 μm %	Silt 2–20 μm %	<2 μm %	<20 μm %	<2000 μm %	Calculated moisture, Fe/Al oxides, and organic matter removed by pretreatment %	ASRIS* classification
MI115	33.1	13.2	33.1	46.3	100	13	Ferrosols
MI120	18.3	8.6	18.3	26.9	100	11	Ferrosols
MI121	16.6	10.1	16.6	26.6	100	6	Ferrosols
MI122	46.1	18.8	46.1	64.9	100	8	Ferrosols
MI124	57.6	17.3	57.6	74.8	100	7	Ferrosols
MI128	22.8	6.7	22.8	29.5	100	6	Ferrosols
MI129	13.1	13.8	13.1	26.9	100	6	Ferrosols
MI132	27.8	11.5	27.8	39.3	100	11	Tenosols

ASRIS* (Australian Soil Resource Information System) [2, 30].

(a) (b)

Figure 1: Example of the Tick Hill landscape for sample sites: (a) MI121 and (b) MI124.

microFTIR 102 [32] (http://www.dpinstruments.com/). Soil samples were oven heated overnight at 60°C to obtain a consistent dryness. MicroFTIR emission measurements were acquired from heated soil samples within ceramic crucibles, also at 60°C, from an approximate 20 mm field of view and using 16 scan integrations. Measurements were calibrated to radiance units ($W/m^2/sr/\mu m$) using hot and cold black body measurements set to 65°C and 30°C, respectively. Background radiance (e.g., "downwelling") was removed by measuring the emission of a brass plate at room temperature (determined via a Pt thermocouple). Temperature-emissivity separation of the acquired radiance measurements was calculated using in-house software developed by CSIRO (Green, *pers. comm.*) to provide absolute emissivity spectral signatures. Each soil sample was also analysed for mineralogy using X-ray diffraction (XRD).

Emission measurements by the microFTIR of each particle size fraction was repeated as a check for slight signature variations when the sample surface was disturbed with a spatula. Only minor changes in absolute emissivity values were observed with no effective change in signature shape. The resulting TIR emissivity signatures were imported into CSIRO software for processing proximal spectral data, "The Spectral Geologist" (TSG, http://www.thespectralgeologist.com/). Interpretation of the emissivity signatures for mineralogy was assisted by comparison with the ASL [26]. Additional spectral measurements of the Tick Hill samples were also undertaken using the PIMA II (Portable Infrared Mineral Analyser; http://www.hyvista.com/) and the Fieldspec FR (http://www.asdi.com/) spectrometers to acquire SWIR reflectance signatures of the Tick Hill raw soil and particle-size fractions.

2.3. ASTER Spectral Library. Fifty one of the soil samples accessible at the ASTER Spectral Library [26] (http://speclib.jpl.nasa.gov/search-1/soil) were used in this study and represented all major soil types. Detailed descriptions and classifications are given for most of the soils, including percentages of sand, silt, and clay provided by the USDA National Soil Survey Laboratory, where clay size is less than 2 μm; silt size ranges from 2 μm to 50 μm; sand size ranges from 50 μm to 2 mm. The USDA system definitions of silt and sand by particle size differ from the International System where silt and sand is defined by particle sizes 2 μm to 20 μm and 20 μm to 2 mm, respectively [2]. This prevented the use of the silt and sand breakdown for the eight Tick Hills samples from being combined with these USDA samples. When available, the USDA determined the clay mineralogy semiquantitatively from the XRD analysis, while mineralogy of the silt and sand was determined

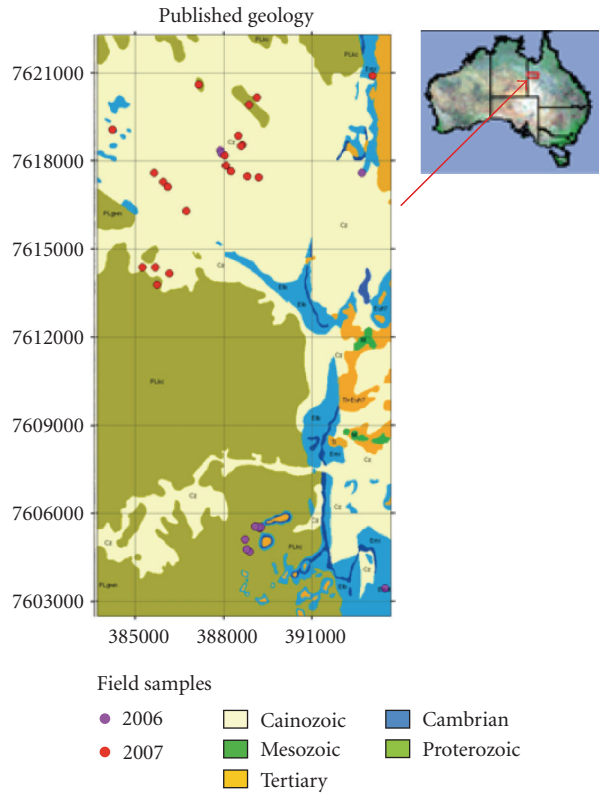

Figure 2: Location of the Tick Hill study area [24], North Queensland, Australia.

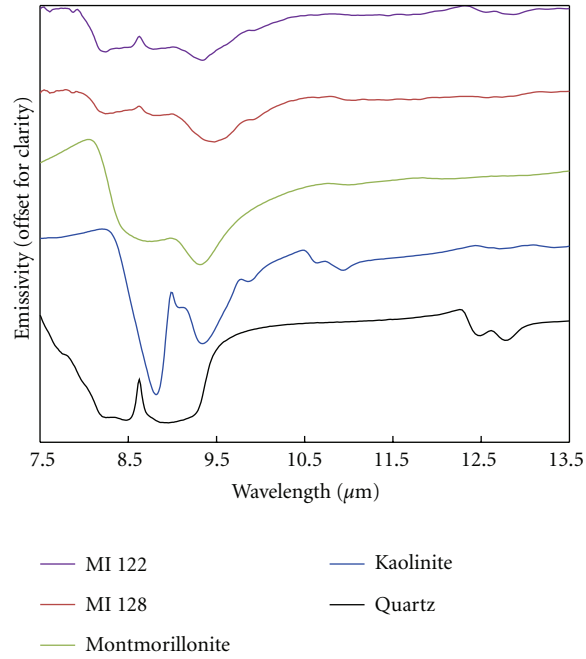

Figure 3: Example MicroFTIR emissivity spectra of Tick Hill soil samples and ASL [26] highlighting the presence of mixtures of clay and quartz minerals within the samples.

by petrographic microscope. The supplied USDA quartz content percentage estimate was recalculated into a total soil quartz content estimate for this study using the clay particle size percentage estimate to derive an adjustment (e.g., Quartz%[silt, sand] $*$ [100 − Clay%]/100). The USDA's percent organic carbon content was also used in this study and obtained by wet combustion analysis [33]. Estimates of quartz contents for the Fowlers Gap samples were derived from normative analysis of soil's XRF elemental results [34]. Particle size analysis of the Fowlers Gap soils was determined using sieving and laboratory techniques assuming USDA system texture classes [34].

The USDA samples included in the ASL were measured for DHR spectra using a Nicolet 5DXB FTIR spectrophotometer at constant 4 cm^{-1} spectral resolution from 2 μm to 14 μm (e.g., SWIR-TIR wavelengths) [35]. A directional (10 degree) hemispherical reflectance attachment was used for measuring a 2.5 cm sample diameter. In this study the ASL TIR signatures were converted from DHR to emissivity, as generated from the microFTIR, assuming Kirchoff's Law [15]. These spectra were also combined with additional 0.4 μm to 2.0 μm spectral measurements for each sample, although the VNIR wavelength region was not studied here.

3. Spectral Analysis and Results

3.1. Tick Hill. XRD analysis of the Tick Hill soils identified minerals such as quartz, smectite, kaolinite, and minor amounts of illite. MicroFTIR emissivity signatures of raw soil samples confirmed the predominance of quartz and clay minerals. In particular, samples MI122 and MI128 indicated the presence of quartz and kaolinite/smectite minerals (Figure 3). Although the quartz "reststrahlen" feature between 8 and 9.5 μm is reduced in the raw soil samples compared to the JHU library spectra, the 8.62 μm feature remains distinctive. Likewise, the 9.0 μm kaolinite feature is less distinctive in the raw soil mixture although the 9.5 μm feature remains.

The corresponding emissivity signatures for the various particle size fractions of samples MI122, and MI128, highlight examples of the trend of an increasing quartz reststrahlen 8.62 μm spectral feature and decreasing clay 9.5 μm feature, with increasing particle size (Figure 4). Also within the 10.5–12 μm wavelength region, "volume" scattering quartz features (QVS) are associated with the 2–20 m and 20–60 μm soil particle fractions [36] (Figure 4).

By comparison, the reststrahlen quartz feature is associated with specular scattering from coarser quartz grains [36]. Several samples, including the displayed MI128, also indicate small amounts of kaolinite within the 2–20 μm and 20–60 μm particle size fractions, as shown by their 9.0 and 9.8 μm spectral features (Figure 4).

The TSG software was customised to target those emissivity features associated with kaolinite/smectite, quartz, and its volume scattering fine-grained variation. In particular, spectral indices were devised to estimate the coarser quartz content, the clay mineral content, and the effects of fine quartz volume scattering; Quartz(ε), Clay(ε), and QVS(ε), respectively. Generally the individual detector bands or

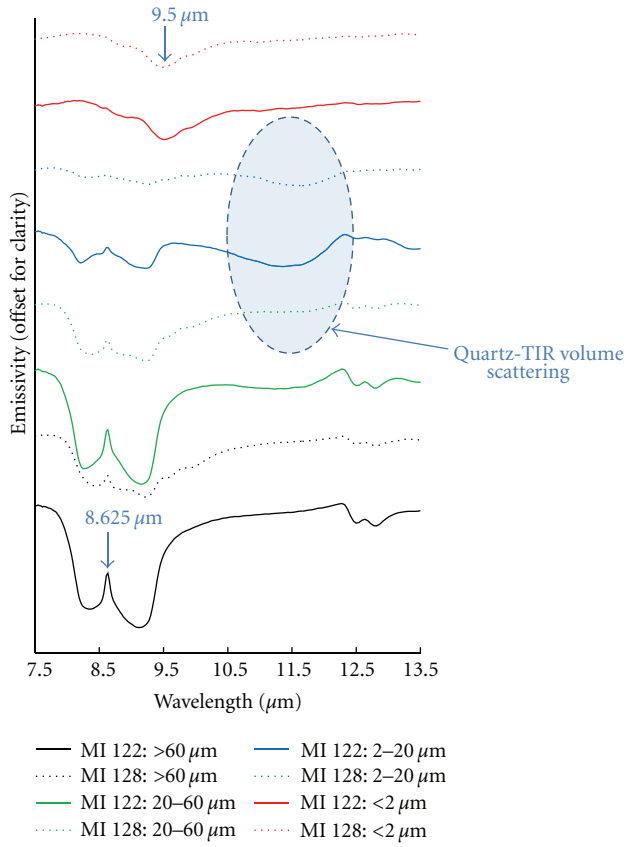

Figure 4: Example MicroFTIR emissivity spectra of particle size separated Tick Hill soil samples showing diagnostic mineral and textural related spectral features.

closest wavelength thereof were used here. These spectral indices were devised to target the spectral absorption feature in a similar method as by [37].

$$\text{Quartz}(\varepsilon) = \frac{2 \times \varepsilon_{(8632)}}{\varepsilon_{8383} + \varepsilon_{8897}}, \quad (1)$$

where $\varepsilon_{(8632)}$ is the mean ε value within ± 30 nm (e.g., between 8602 and 8664 nm), and ε_{8383} and ε_{8897} are the ε values at wavelengths 8383 and 8897 nm, respectively.

Figure 5 highlights these wavelengths in relation to the quartz reststrahlen spectral feature. The estimation of quartz content using (1), as a spectral index based on the diagnostic reststrahlen absorption feature, follows examples of the previous application of spectral indices with proximal and airborne hyperspectral data [23, 24].

Similarly, indices were devised for Clay (kaolinite) and estimates of the quartz volume scattering effect.

$$\text{Clay}(\varepsilon) = \frac{\varepsilon_{9178} + \varepsilon\varepsilon_{9852}}{2 \times \varepsilon_{9500}}, \quad (2)$$

$$\text{QVS}(\varepsilon) = \frac{\varepsilon_{10318} + \varepsilon_{12279}}{\varepsilon_{11320} + \varepsilon_{11664}}. \quad (3)$$

The results of these spectral indices for each Tick Hill soil fraction, processed using TSG, are shown in Figures 6, 7, and 8. Figure 6 indicates an approximate increasing trend in the quartz spectral parameter with increasing grain size. A higher quartz volume scattering behaviour for the mid-sized fractions (e.g., 2–60 μm) is shown by the auxiliary colour coding (green to red, Figure 6) for the sample points. Figure 7 shows a clear inverse trend between the clay and quartz spectral indices. However a high clay value can still appear within silty fractions (e.g., cyan coding, Log ~1.0 or ~10 μm) and some coarser fractions (e.g., red) exhibit a high clay spectral index. The Clay(ε) versus Quartz(ε) relationship shown in Figure 7 shows a high correlation of determination (R^2) value of 0.85. Although it should be noted that this dataset included repeated microFTIR measurements for each sample fraction. Developing predictive clay% algorithms is complicated by such residual clay mineral content within the separated soil fractions. However Figure 8 suggests predicting clay mineral content within fractions finer than 10 μm with low quartz content (e.g., blue) is possible.

A spectral index was determined for the SWIR spectral measurements collected using the PIMA II. A TSG-based algorithm calculating the depth of a 4th-order polynomial at the 2.2 μm clay absorption feature was applied to continuum-removed spectra ("clay/kaolinite (SWIR)") for all Tick Hill soil particle fractions (Figures 9(a) and 9(b)). The value of clay/kaolinite (SWIR) was set to 0 when no 2.2 μm SWIR absorption feature was identified. Comparing the SWIR and TIR mineral clay indices for all the Tick Hill fractions showed a broad range of values (Figure 9(a)). However a better correlation between particle size and TIR-derived mineral Clay(ε) index was apparent when only the three <2 μm, 2–20 μm and 20–60 μm fractions were examined (Figure 9(b)). It appears likely that there is some contamination of clay mineral content within the coarser fractions, possibly as a coating to the grains. This was suggested by examples of clay spectral features (e.g., MI128 fractions, Figure 4).

Applying these spectral indices to the eight natural Tick Hill soil samples did not reveal clear relationships with texture although the number of samples was small. The mineral Clay(ε) index versus lab derived clay content for these natural samples (Figure 10) clearly indicated a much larger population and range of soil samples is required to test the application of these spectral techniques, as further investigated in the following section.

3.2. ASTER Spectral Library Soils. SWIR and TIR spectral signatures of 51 soils from the ASL [26] were included in this study to evaluate the devised spectral indices for composition and texture of natural soil samples. Examples of these ASL USDA and Fowlers Gap spectral signatures are shown in Figures 11(a) and 11(b), respectively. These spectra highlight the diverse range of soil environments represented, including organic-rich Spodosol loam (874264), aeolian based sandy Alfisol loam (87P2376), micaceous Inceptisol loam (88P2535), and quartz rich alluvial Entisol sand (FGG027) (Figures 11(a) and 11(b)).

The same spectral indices as described in (1)–(3) were applied to the ASL soil spectra using Excel rather than TSG in this application. Differences between the ASL Nicolet

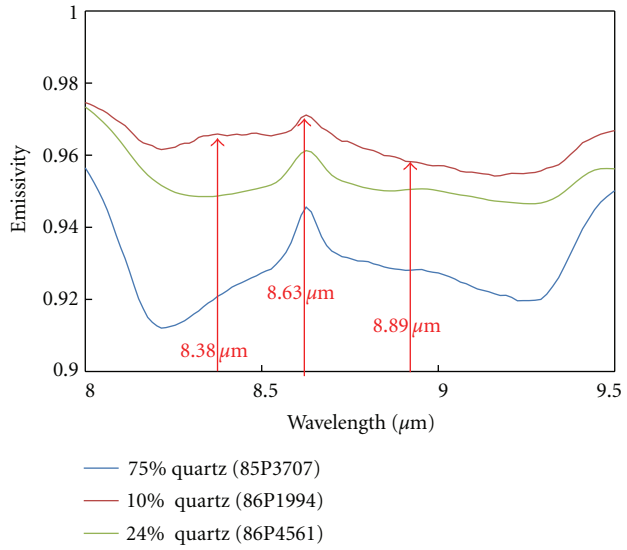

Figure 5: Examples of USDA TIR soil signatures of variable quartz content (XRD analysis of silt-sand fraction) in relation to the diagnostic 8.63 μm reststrahlen feature.

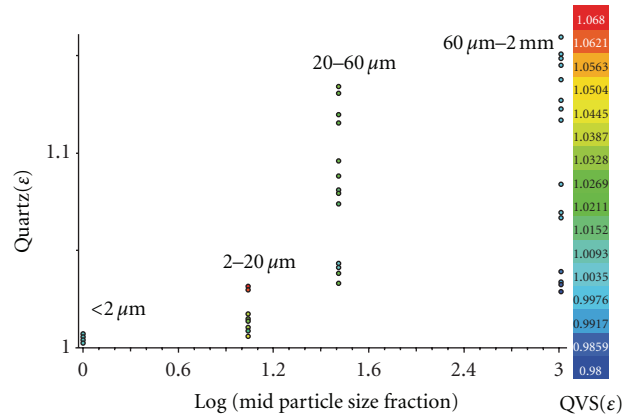

Figure 6: Quartz content spectral index (Quartz(ε)) versus log of the particle size fraction and colour coded by the fine quartz volume scattering (QVS(ε) (e.g., red = high scattering associated with fine quartz), showing an approximate decrease in quartz content with decreased grain size.

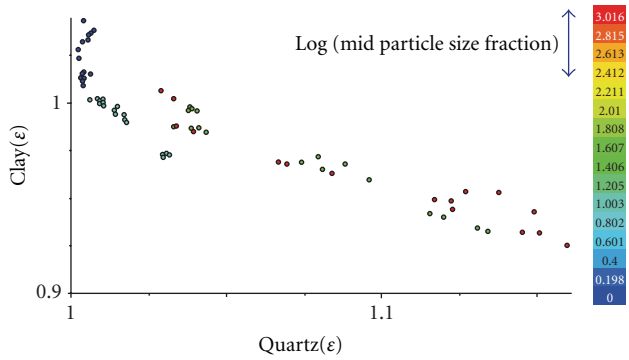

Figure 7: Relationship between quartz and clay content spectral parameters colour coded by the log of the particle size (e.g., red >2.8 or ~60 μm–2 mm; blue <1 or ~<2 μm), showing the inverse relationship between TIR interpreted quartz and clay mineral contents.

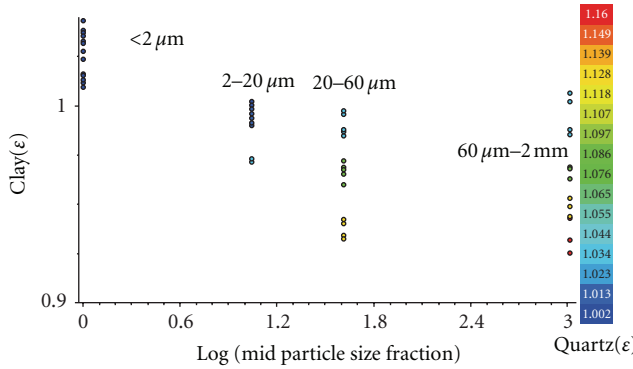

Figure 8: Relationship between the clay content spectral parameter and the log of the particle size colour coded by the quartz content spectral parameter (e.g., low quartz content: blue, high quartz: red).

5DXB FTIR and the CSIRO-ESRE MicroFTIR measurements required a slight adjustment of the spectral indices although the differences in the TIR wavelengths were minor.

A distinct SWIR absorption feature at 2.2 μm (e.g., 2200 nm) can be observed for several of AlOH clay and phyllosilicate minerals that could comprise the clay fine particle fraction of soils (e.g., montmorillonite, kaolinite, and muscovite, Figure 12). A relative band depth index, AlOH RBD(ρ), was devised for this 2200 nm feature to discriminate such clay minerals (Figure 12) by (4)

$$\text{AlOH RBD}(\rho) = \frac{\rho_{2100} + \rho_{2300}}{\rho_{2195} + \rho_{2215}}, \quad (4)$$

where ρ_{2100} is the reflectance value at 2100 nm, and so forth.

In particular, (4) uses an average estimate of the absorption spectral feature at 2195 and 2215 nm as the denominator and the shoulders of the absorption at 2100 and 2300 nm for the numerator as a variation of the relative band depth technique.

Both the Clay(ε) and AlOH RBD(ρ) indices for the combined Tick Hill and ASL data sets show no coherent correlation between clay mineralogy and clay particle size despite the use of an enlarged sample population of soils with a wider range in clay content (Figure 13).

The poor result for the spectrally derived clay content% (Figure 13) could be due to a number of factors including (1) interference from the 8 to 9.2 μm quartz reststrahlen feature on the 9.5 μm clay absorption-based spectral index, (2) limitations of the relative band depth spectral algorithm applied for clay/AlOH mineral content, (3) nonlinear effects from multiple scattering between clay mineral particles coating coarser grain particles, or (4) the presence of fine nonclay mineral particles less than 2 μm distorting the measured clay fraction (e.g., iron oxides, organics). A variation of the clay (ε) spectral index, calculated using (2), was

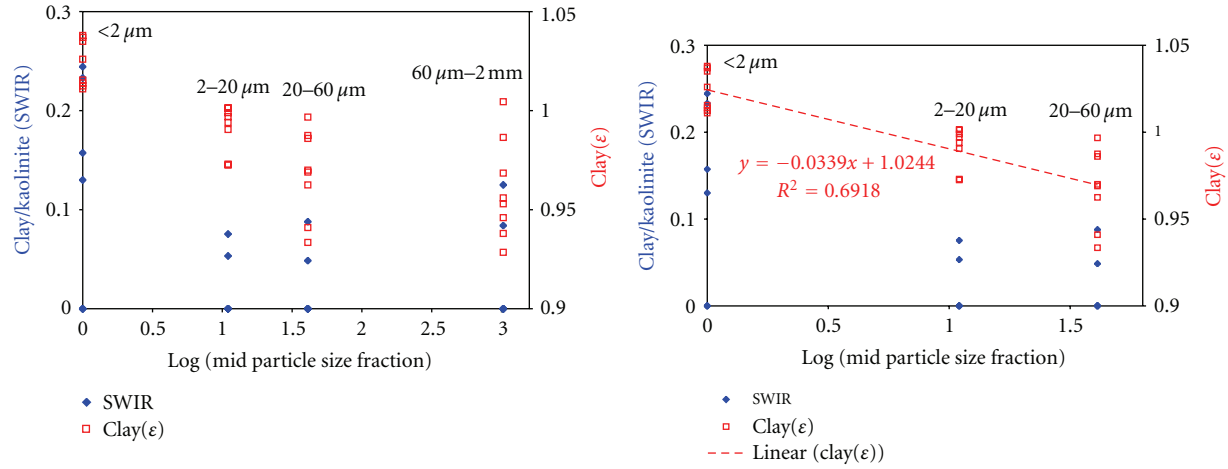

(a) (b)

Figure 9: (a) Comparison of clay mineral content determined by SWIR defined clay/kaolinite spectral index and TIR defined Clay(ε) for the four Tick Hill particle size fractions. (b) Close up of (a) and line of best fit for Clay(ε) results for finest three particle size fractions.

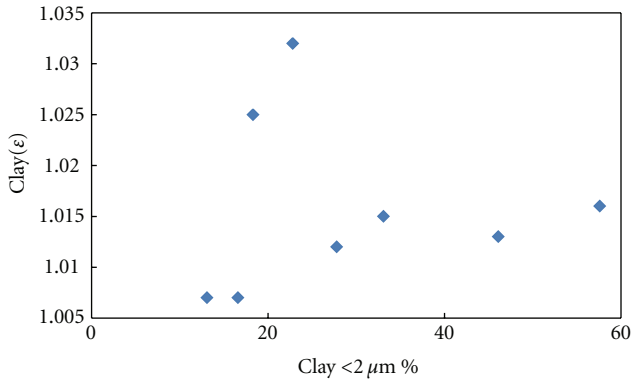

Figure 10: TIR-derived Clay(ε) mineral index versus the particle size determined clay% of the eight natural Tick Hill samples.

subsequently generated using the 9.0 μm kaolinite spectral feature, that remains even with the dominant presence of quartz (Figure 3) and described here in (5):

$$\text{Clay2}(\varepsilon) = \frac{2 \times \varepsilon_{9000}}{\varepsilon_{8862} + \varepsilon_{9257}}. \quad (5)$$

However the resulting Clay2(ε) index also produced a poor result showing no effective correlation with the USDA clay content%.

The results of the Quartz(ε) compared to the petrographic determination of quartz content associated with the USDA soil spectra indicated a relationship involving a power function ($n = 2$) with a moderate coefficient of determination, $R^2 = 0.69$ (Figure 14). Including the Fowlers Gap soils into this sample population did not alter this R^2 result significantly. However the Fowlers Gap quartz content was derived from a different method involving a normative

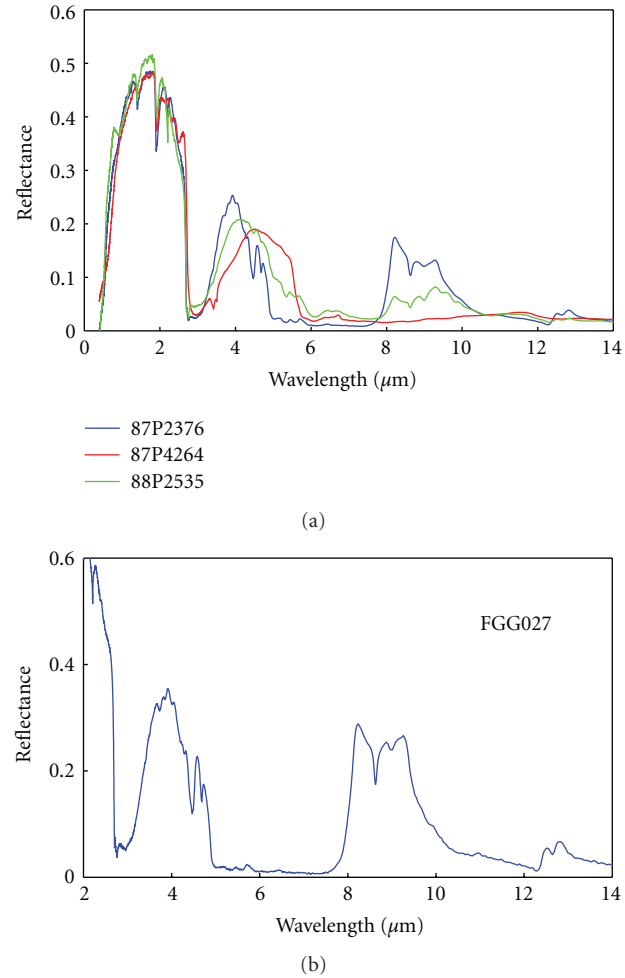

(a)

(b)

Figure 11: (a) Examples from the USDA soil spectra included within the ASL. (b) Example from the semiarid Fowlers Gap (Australia) included in the ASL [26].

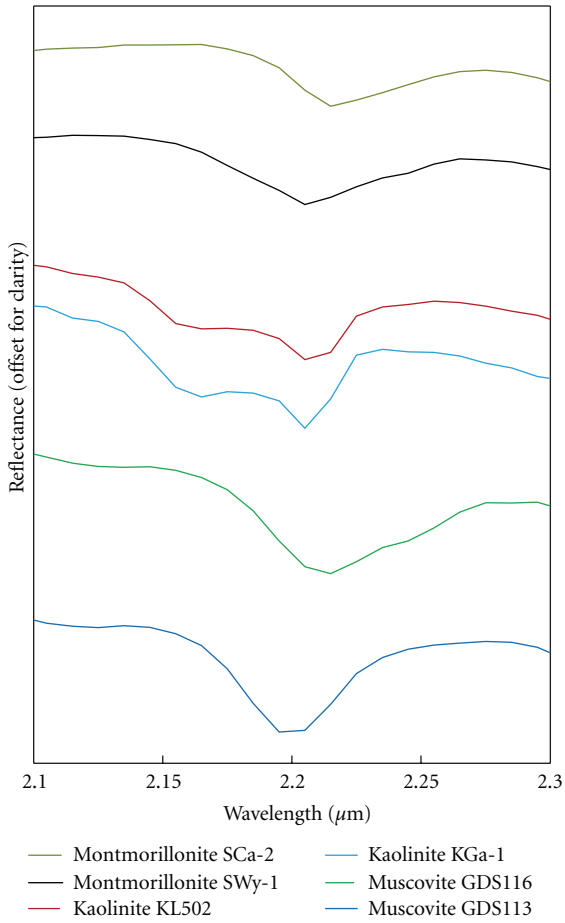

Figure 12: USGS VNIR-SWIR mineral library reflectance signatures for AlOH or clay phyllosilicate minerals highlighting the main 2.2 μm absorption spectral feature [12].

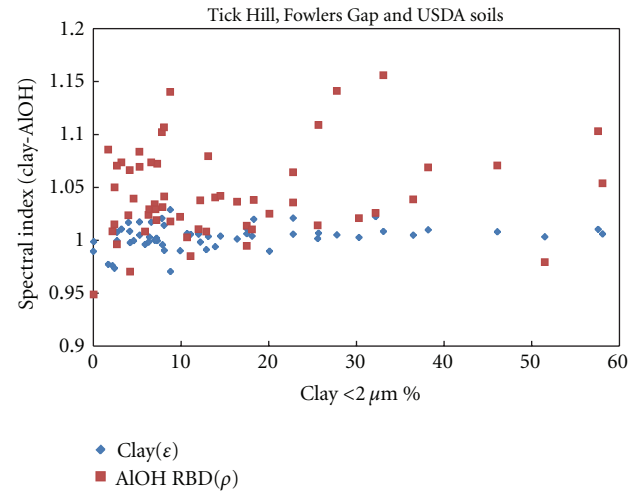

Figure 13: Comparison between the SWIR derived, AlOH RBD(ρ), and TIR derived, Clay(ε), mineral spectral indices, and the clay particle size content supplied by USDA.

calculation based on XRF elemental analysis, and therefore not necessarily consistent with the USDA results.

The quartz volume scattering index (QVS) showed some minor increasing trend with silt content% for the USDA and Fowlers Gap samples, however the R^2 was a low 0.27. This index appears to be of more potential interest for the study of separated soil fractions than for natural soil samples.

Attempts were also undertaken to derive nonmineral organic carbon soil composition from the ASL soil spectra, using spectral indices calculated from MIR absorption features and USDA determined organic carbon results. An examination of several USDA soil DHR spectra revealed organic carbon features at 3.41 μm ("A") and 3.5 μm ("B") (Figure 15). Note that the displayed USDA soil, 874264, is an organic-rich Spodosol loam containing the highest organic carbon of 28% within the ASL sample collection. These MIR DHR spectra (also shown in Figure 11(a)) highlight the processing between 3.3 μm and 3.6 μm where the hull continuum removal acts as normalisation process [38] and simplifies the calculation of spectral indices as absorption depths (Figure 15).

Several depth indices were devised, centred at 3.41 and 3.5 μm features as included in (6)–(8):

$$\text{MIR organic hull depth A} = 1 - \rho_{(3415)}, \tag{6}$$

where $\rho_{(3415)}$ is the mean ρ value within ± 10 nm (e.g., between 3405 to 3425 nm)

$$\text{MIR organic hull depth B} = 1 - \rho_{(3490)}, \tag{7}$$

where $\rho_{(3490)}$ is the mean ρ value within ± 15 nm (e.g., between 3475 and 3505 nm)

$$\begin{aligned}\text{MIR organic hull depth average} &= \text{MIR organic hull depth A} \\ &+ \text{MIR organic hull depth A.}\end{aligned} \tag{8}$$

In addition, a spectral index was derived from the area bounded by the hull (=1 in Figure 15) and the spectral signature between 3.3 and 3.6 μm. This required a reversal of the hull signatures and calculation of area under the resulting curve. The highest "correlation" of the four indices to the USDA organic carbon estimates was achieved using the MIR organic carbon depth index A, R^2 of 0.53 (Figure 16(a)). However this included an extreme outlying sample containing 28% organic carbon and the correlation reduced to a R^2 of 0.39 when this was omitted (Figure 16(b)). Likewise, the MIR organic hull average depth and Areal based indices produced a R^2 of 0.37 and $R^2 = 0.34$, respectively, that reduced to R^2 values of 0.19 and 0.18, respectively, when this single outlying high organic carbon sample was excluded. Although these preliminary results showed no coherent correlation, this outcome would be confirmed if more soils were included containing a greater range of organic carbon between 10 and 30%. However, as the majority of terrestrial soils contain less than 10% organic carbon, its determination using such spectral indices appears unlikely. Figure 17 also

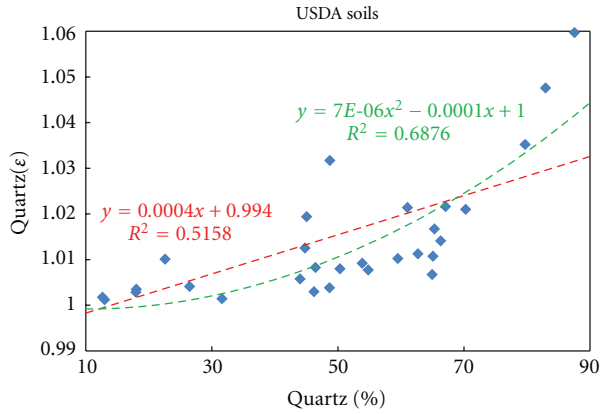

Figure 14: Comparison between the Quartz(ε) and USDA determined quartz% content with calculated linear (red) and power relation (green) models.

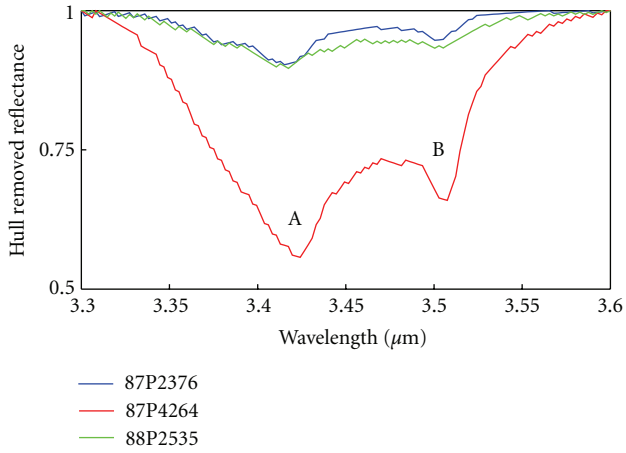

Figure 15: Examples of hull removed 3.3 μm to 3.6 μm ASL reflectance spectra (see Figure 11(a)) highlighting organic carbon spectral absorption features at 3.41 μm ("A") and 3.5 μm ("B") applied to several USDA soil samples.

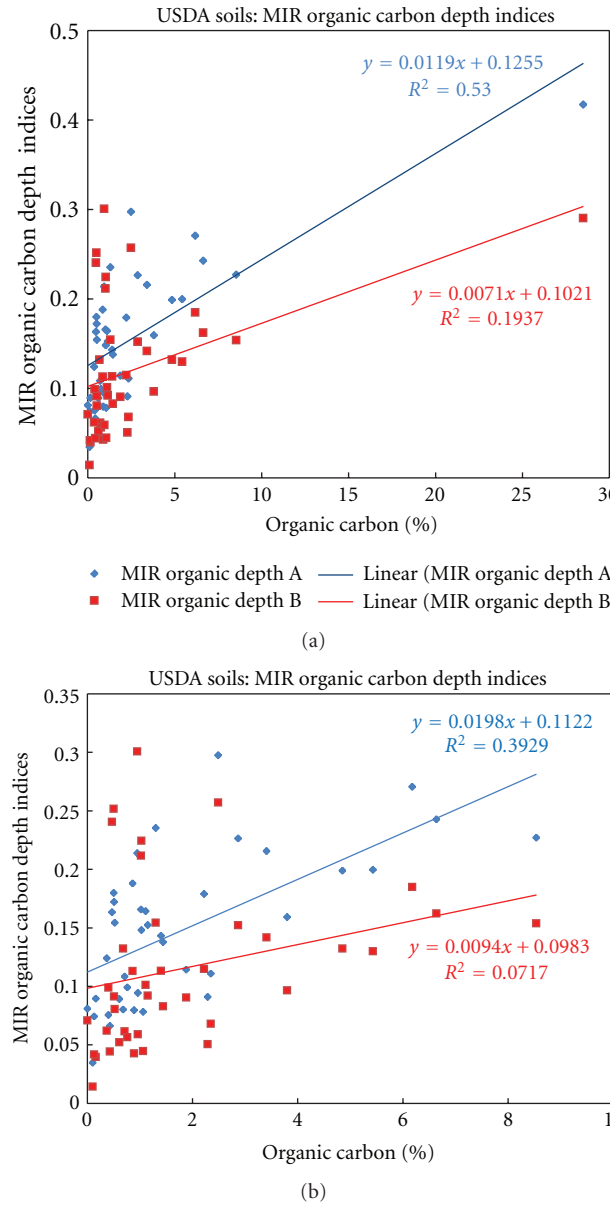

Figure 16: MIR organic carbon depth indices A and B versus the USDA organic carbon content; (a) for all data; (b) omitting outlying organic carbon rich sample at 28%.

shows this limitation with the MIR organic hull depth average Index result for values between 0 and 10% organic carbon.

4. Conclusions

The study of the particle size fractions derived from Tick Hill soil samples show the intimate connection between mineralogy and texture when examining TIR spectra. In particular, coarse and fine-grained quartz components have distinct TIR spectral features. The spectral results also indicate that residual clay minerals may still be present in the sand fraction, even with thorough particle size separation processes, and potentially bias the determination of "clay" content if based on sedimentation analysis alone (e.g., <2 μm). The proximal spectral measurements of Tick Hill samples suggested its potential to analyse for clay mineral content. In particular, the Tick Hill results suggested that a TIR spectral index based on the 9.5 μm absorption feature is useful for the determination of clay content within soil particle size fractions.

Further investigations using a larger population of natural soil samples, available from the ASL, showed no strong correlations between laboratory-determined clay particle size and the clay derived from either SWIR or TIR based spectral indices. Possible causes for this may be (1) interference from the 8 to 9.2 μm quartz reststrahlen feature on the 9.5 μm and 9.0 μm clay absorption based spectral indices, (2) limitations of the spectral relative band depth algorithm, (3) nonlinear effects from clay mineral particle coatings over coarser grain particles, or (4) the presence of nonclay mineral particles

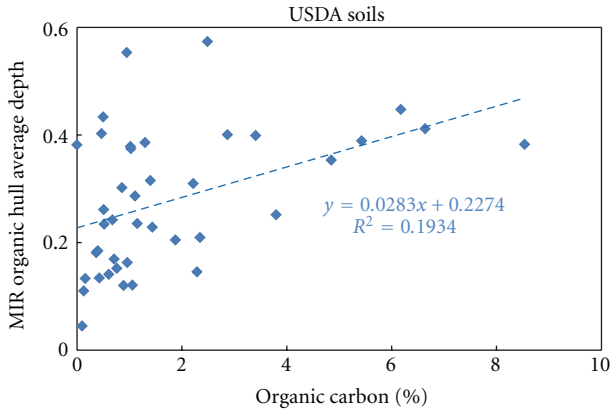

Figure 17: MIR organic hull average depth index versus the USDA supplied Organic Carbon content for organic carbon less that 10% content.

finer than 2 μm but included within the "clay" particle fraction. A moderate nonlinear correlation was indicated between the TIR quartz derived index, based on the 8.62 μm reststrahlen feature, and the petrographic-derived quartz content. Preliminary efforts were also undertaken to derive an organic carbon spectral index using absorption features between 3.4 and 3.5 μm associated with the fundamental H–C stretching vibration bands. No strong correlations with the USDA organic carbon estimates were apparent using hull continuum removed spectra to provide indices based on depth and area of the absorption features.

Acknowledgments

Adrian Beech, former manager of Analytical Services, CSIRO Land and Water, is sincerely thanked for undertaking the extensive particle size analysis and sample separation of the Tick Hill soils. Assistance from Peter Mason of CSIRO has also been helpful in the application of TSG software. Encouragement and support from Vittala Shettigara of DSTO, Simon Hook of JPL, Simon Jones of RMIT, Alan Marks, and Ian Goicoechea is also gratefully appreciated. Matilda Thomas publishes with the permission of the Chief Executive Officer of Geoscience Australia.

References

[1] R. P. C. Morgan, *Soil Erosion and Conservation*, Blackwell, Malden, Mass, USA, 3rd edition, 2005.

[2] R. E. White, *Principles and Practice of Soil Science—The Soil as a Natural Resource*, Blackwell, Malden, Ma, USA, 4th edition, 2006.

[3] C. Kosmas, M. Kirkby, and N. Geeson, "Manual on: Key indicators of desertification and mapping environmentally sensitive areas to desertification," EUR 18882, European Commission, Energy, Environment and Sustainable Development, 1999.

[4] Food and Agriculture Organisation of the United Nations, *The State of Food Insecurity in the World*, Rome, Italy, 2011.

[5] E. Ben-Dor, S. Chabrillat, J. A. M. Demattê et al., "Using imaging spectroscopy to study soil properties," *Remote Sensing of Environment*, vol. 113, no. 1, pp. S38–S55, 2009.

[6] J. A. Hackwell, D. W. Warren, R. P. Bongiovi, S. J. Hansel, T. L. Hayhurst, and D. J. Mabry, "LWIR/MWIR imaging hyperspectral sensor for airborne and ground-based remote sensing," in *Imaging Spectrometry II*, vol. 2819 of *Proceedings of the SPIE*, pp. 102–107, 1996.

[7] S. Achal, J. E. McFee, T. Ivanco, and C. Anger, "A thermal infrared hyperspectral imager (TASI) for buried landmine detection," in *Detection and Remediation Technologies for Mines and Minelike Targets 7*, vol. 6553 of *Proceedings of SPIE*, The International Society for Optical Engineering, April 2007.

[8] J. W. Salisbury and D. M. D'Aria, "Infrared (8–14 μm) remote sensing of soil particle size," *Remote Sensing of Environment*, vol. 42, no. 2, pp. 157–165, 1992.

[9] J. W. Salisbury and D. M. D'Aria, "Emissivity of terrestrial materials in the 8–14 μm atmospheric window," *Remote Sensing of Environment*, vol. 42, no. 2, pp. 83–106, 1992.

[10] C. D. Elvidge, "Thermal infrared reflectance of dry plant materials: 2.5–20.0 μm," *Remote Sensing of Environment*, vol. 26, no. 3, pp. 265–285, 1988.

[11] J. W. Salisbury and D. M. D'Aria, "Emissivity of terrestrial materials in the 3–5 μm atmospheric window," *Remote Sensing of Environment*, vol. 47, no. 3, pp. 345–361, 1994.

[12] R. N. Clark, T. V. V. King, M. Klejwa, G. A. Swayze, and N. Vergo, "High spectral resolution reflectance spectroscopy of minerals," *Journal of Geophysical Research*, vol. 95, no. 8, pp. 12653–12680, 1990.

[13] R. H. Merry and L. J. Janik, "Mid infrared spectroscopy for rapid and cheap analysis of soils," in *Proceedings of the 10th Australia Agronomy Conference*, January 2001.

[14] R. A. Viscarra Rossel, D. J. J. Walvoort, A. B. McBratney, L. J. Janik, and J. O. Skjemstad, "Visible, near infrared, mid infrared or combined diffuse reflectance spectroscopy for simultaneous assessment of various soil properties," *Geoderma*, vol. 131, no. 1-2, pp. 59–75, 2006.

[15] J. W. Salisbury, A. Wald, and D. M. D'Aria, "Thermal-infrared remote sensing and Kirchhoff's law—1. Laboratory measurements," *Journal of Geophysical Research*, vol. 99, no. 6, pp. 11897–11911, 1994.

[16] W. C. Snyder, Z. Wan, Y. Zhang, and Y. Z. Feng, "Thermal infrared (3–14 μm) of bidirectional reflectance measurements of sands and soils," *Remote Sensing of Environment*, vol. 60, no. 1, pp. 101–109, 1997.

[17] R. D. Hewson, G. R. Taylor, and L. B. Whitbourn, "Application of TIR imagery and spectroscopy for the extraction of soil textural information at fowlers gap, Western New South Wales, Australia," in *Proceedings of the IEEE International Geoscience and Remote Sensing Symposium*, pp. 723–726, July 2008.

[18] J. A. Sobrino, J. C. Jiménez-Muñoz, L. Balick, A. R. Gillespie, D. A. Sabol, and W. T. Gustafson, "Accuracy of ASTER Level-2 thermal-infrared standard products of an agricultural area in Spain," *Remote Sensing of Environment*, vol. 106, no. 2, pp. 146–153, 2007.

[19] G. Hulley and S. Hook, *HyspIRI Level-2 Thermal Infrared (TIR) Land Surface Temperature and Emissivity Algorithm Theoretical Basis Document*, JPL Publication 11-5, Jet Propulsion Laboratory, NASA, Pasadena, Calif, USA, 2011.

[20] Z. L. Li, F. Becker, M. P. Stoll, and Z. Wan, "Evaluation of six methods for extracting relative emissivity spectra from thermal infrared images," *Remote Sensing of Environment*, vol. 69, no. 3, pp. 197–214, 1999.

[21] A. Mushkin, L. K. Balick, and A. R. Gillespie, "Extending surface temperature and emissivity retrieval to the mid-infrared (3–5 μm) using the Multispectral Thermal Imager (MTI)," *Remote Sensing of Environment*, vol. 98, no. 2-3, pp. 141–151, 2005.

[22] L. Kirkland, K. Herr, E. Keim et al., "First use of an airborne thermal infrared hyperspectral scanner for compositional mapping," *Remote Sensing of Environment*, vol. 80, no. 3, pp. 447–459, 2002.

[23] T. J. Cudahy, M. Caccetta, A. Cornelius et al., "Regolith geology and alteration mineral maps from new generation airborne and satellite remote sensing technologies; and Explanatory Notes for the Kalgoorlie-Kanowna, 1:100,000 scale map sheet, remote sensing mineral maps," MERIWA Report 252, Perth, Australia, 2005.

[24] T. Cudahy, M. Jones, M. Thomas et al., *Mapping Soil Surface Mineralogy at Tick Hill, North-Western Queensland, Australia, Using Airborne Hyperspectral Imagery*, Springer, 1st edition, 2010.

[25] R. Hewson, T. Cudahy, A. Beech, M. Jones, and M. Thomas, "Mineral and textural investigations of soils using thermal infrared spectroscopy," in *Proceedings of the 19th World Congress of Soil Science*, Brisbane, Australia, August 2010.

[26] A. M. Baldridge, S. J. Hook, C. I. Grove, and G. Rivera, "The ASTER spectral library version 2.0," *Remote Sensing of Environment*, vol. 113, no. 4, pp. 711–715, 2009.

[27] J. A. Sobrino, C. Mattar, P. Pardo et al., "Soil emissivity and reflectance spectra measurements," *Applied Optics*, vol. 48, no. 19, pp. 3664–3670, 2009.

[28] R. D. Hewson and G. R. Taylor, "An investigation of the geological and geomorphological features of Fowlers Gap using thermal infrared, radar and airborne geophysical remote sensing techniques," *Rangeland Journal*, vol. 22, no. 1, pp. 105–123, 2000.

[29] N. J. McKenzie, K. J. Coughlan, and H. P. Cresswell, *Soil Physical Measurement and Interpretation for Land Evaluation*, CSIRO Publishing, Melbourne, Australia, 2002.

[30] R. F. Isbell, *The Australian Soil Classification*, CSIRO, Melbourne, Australia, 1996.

[31] P. Carlile, E. Bui, C. Moran, D. Simon, and B. Henderson, "Method used to generate soil attribute surfaces for the Australian Soil Resource Information System using soil maps and look-up table ," CSIRO Land and Water Technical Report 24/01, CSIRO, 2011.

[32] S. J. Hook and A. B. Kahle, "The micro Fourier Transform Interferometer (μFTIR)—a new field spectrometer for acquisition of infrared data of natural surfaces," *Remote Sensing of Environment*, vol. 56, no. 3, pp. 172–181, 1996.

[33] A. Walkley and I. A. Black, "An examination of the Degtjareff method for determining organic carbon in soils: effect of variations in digestion conditions and of inorganic soil constituents," *Soil Science*, vol. 63, pp. 251–263, 1934.

[34] R. D. Hewson, L. B. Whitbourn, and G. R. Taylor, "Application of TIMS imagery and airborne CO2 laser spectroscopy for geological and geomorphological investigations in an arid environment, Western NSW, Australia," in *Proceedings of the 12th International Conference of Applied Geologic Remote Sensing*, vol. 2, pp. 373–384, 1997.

[35] J. W. Salisbury, D. M. D'Aria, and L. E. Brown, *Infrared (2.08–14 μm) Spectra of Soils: A Preliminary Report*, Department of Earth and Planetary Sciences, Johns Hopkins University, 1990.

[36] J. W. Salisbury and J. W. Eastes, "The effect of particle size and porosity on spectral contrast in the mid-infrared," *Icarus*, vol. 64, no. 3, pp. 586–588, 1985.

[37] J. K. Crowley, D. W. Brickey, and L. C. Rowan, "Airborne imaging spectrometer data of the Ruby Mountains, Montana: mineral discrimination using relative absorption band-depth images," *Remote Sensing of Environment*, vol. 29, no. 2, pp. 121–134, 1989.

[38] F. Van Der Meer, "Spectral curve shape matching with a continuum removed CCSM algorithm," *International Journal of Remote Sensing*, vol. 21, no. 16, pp. 3179–3185, 2000.